J. Fluid Mech. (1975), *vol.* 70, *part* 1, *pp.* 89–112
Printed in Great Britain

Thermal convection in gas–droplet mixtures with phase transition

By T. KAMBE

Institute of Space and Aeronautical Science, University of Tokyo, Komaba, Meguro-ku, Tokyo, Japan

AND R. TAKAKI

Faculty of General Education, Tokyo University of Agriculture and Technology, Fuchu-shi, Tokyo, Japan

(Received 29 December 1972 and in revised form 9 October 1974)

Thermal convection in a three-component fluid consisting of an inert carrier gas, a condensable vapour and small liquid droplets dispersed throughout the gaseous components has been investigated both theoretically and experimentally. The theoretical study is concerned with the stability of a horizontal fluid layer subject to gradients of both temperature and droplet density. The stability is characterized by four parameters: two material constants, that is, a modified Prandtl number P and a constant Q proportional to $D_m - \kappa$ (D_m is the mutual mass diffusivity of the two gaseous constituents, κ the thermometric conductivity of the gas phase), a modified Rayleigh number R and a parameter S defined as the ratio of the droplet density gradient to the gas density gradient. It is shown for positive R that, irrespective of the value of R, the system is stable for $S > S_\infty$ (S_∞ is a constant dependent on P and Q) and unstable for $S < Q$ (Q is normally less than S_∞) and that for the intermediate range $Q < S < S_\infty$ a transition from stability to instability occurs via an oscillatory state as R is increased through a critical value depending on S. It is shown that the stability is governed largely by both vapour diffusion through the inert gas and droplet growth or decay due to phase changes.

In the experiments, thermal convection in a three-component fluid consisting of air, water vapour and water droplets was investigated. The cloud of droplets was mainly formed by injecting cigarette smoke into a horizontal layer of air saturated with water vapour. After the injection several phases of motion were observed successively. Among them there were travelling waves and steady cellular convection. Measurements were made of the critical Rayleigh numbers for the onset of the phases, the scale of the steady convection cells and the speed of the travelling waves. It is found that all the qualitative features of the experiment are explained by the theory.

1. Introduction

The subject of this paper is thermal convection in a horizontal layer of a three-component fluid consisting of an inert carrier gas, a condensable vapour and

droplets of the liquid phase of this vapour dispersed throughout the gaseous components. It is well known that a simple (one-component) fluid heated from below becomes unstable and exhibits convective motion at a sufficiently large temperature gradient. However, past evidence suggests that in atmospheric convection the evaporation and condensation of water vapour have a large effect on the motion. Many laboratory experiments concerning this mechanism have been made, using various methods to simulate the heat production due to phase changes. Turner (1963) used a combination of two liquids which releases small gas bubbles through a chemical reaction and observed the development of thermals. The density increase produced by mixing water and alcohol was adopted by Turner & Yang (1963) in order to simulate the turbulent mixing at a cloud top. This method was also used by Yang (1968). In the experiments of Hadlock & Hess (1968) heat production by chemical reaction was employed. Cellular convection patterns in a fluid with internal heat production by an electric current were observed by Tritton & Zarraga (1967) and Schwiderski & Schwab (1971). In the experiments cited above, attention was given mainly to the effect of heat production by phase changes in atmospheric convection. However, since the convective motion in the atmosphere often takes place in a three-component fluid (consisting of air, water vapour and droplets), it may be worthwhile to examine to what extent the motion is affected by the following three effects: mutual diffusion between the vapour and the inert gas, the gradient of the distribution of liquid droplets and temperature differences between the gas and liquid phases.

The stability problem of a fluid layer having gradients of two properties was first studied in order to clarify thermal convection in the ocean: to elucidate the phenomenon called 'thermohaline convection', where the relevant properties are temperature and salt concentration. Stommel, Arons & Blanchard (1956) first noted some of its properties, including the 'salt fountain'. The system was analysed by Stern (1960), who noted the general features of the phenomenon now commonly known as 'salt fingers'. Turner (1973) gave a comprehensive review of convection in two-component fluids under the title 'Double-diffusive convection'. Another multidiffusive problem was discussed by Schechter, Prigogine & Hamm (1972), who studied the effect of thermal diffusion on the convective instability of a two-component fluid layer. Wollkind & Frisch (1971) studied the thermal instability of a layer of dissociating fluid, taking into account the effect of mutual diffusion on the instability, where the role of dissociation energy is analogous to that of latent heat liberated through phase changes.

Since in our system there are gradients of three properties, i.e. temperature, vapour density and droplet mass fraction, the thermal convection is expected to be modified in a substantial manner by the four effects mentioned above and to have new characteristics. The dynamics of a three-component fluid can be formulated by an extension of the work of Marble (1969), who dealt with a two-component fluid consisting of a vapour and droplets of its liquid phase. In order to simplify our analysis we employ the following fluid model, which approximates a real state in the laboratory experiment described below.

(*a*) We make a Boussinesq-like approximation, i.e. it is assumed that the fluid

behaves as an incompressible one and density differences can be neglected except in the buoyancy term in the momentum equation. According to Spiegel & Veronis (1960), this approximation is applicable if the vertical dimension of the fluid is much less than the scale heights associated with the static distributions of temperature, pressure and density, and if the fluctuations in temperature, pressure and density do not exceed, in order of magnitude, their total variations in the static state. These conditions are assumed to be satisfied.

(*b*) The distribution of liquid droplets is assumed to be sufficiently dense that evaporation (or condensation) takes place everywhere in the fluid, but individual droplets are regarded as non-interacting. In other words, the droplet radius is assumed to be small enough to satisfy these two requirements. We neglect the diffusion of droplets by Brownian motion because the corresponding diffusivity is normally much less than molecular diffusivities such as the kinematic viscosity or the thermometric conductivity (see the first paragraph of appendix A). Since the droplets are small, their sedimentation is neglected. Thus the droplets are assumed to be merely convected by the surrounding gas, and their velocity relative to the gas is neglected.

(*c*) The characteristic time of the thermal convection is assumed to be much larger than those associated with various relaxation phenomena among the three components. If there is a bounding wall, it is assumed to be wet. Therefore we may regard the fluid system as being in quasi-equilibrium, and the vapour as being nearly saturated. It is also assumed that the inert gas and the vapour have a common temperature distribution, which may be slightly different from that of the droplets since condensation of vapour on them releases latent heat.

(*d*) We assume that the vapour and the droplet densities are much smaller than the inert-gas density. By this assumption the effect of mutual diffusion between the two gaseous components is neglected except in the continuity equation of the vapour.

Under these assumptions, the linear perturbation equations are reduced to three equations closely similar in form to those for the two-component case (equations (8.1.3) and (8.1.4) of Turner 1973). The remarkable difference from that case is the existence (when the diffusion of droplets is neglected) of an absolute instability independent of Rayleigh number for some droplet distributions. The limits of the regions of instability depend on the relative magnitude of the coefficients of heat and vapour diffusion through the inert gas. If the coefficient of vapour diffusion is larger than that of heat, in other words, if the vapour diffuses more rapidly than heat, a layer heated from below becomes absolutely unstable if the (stable) gradient of the droplet distribution is less than a certain limit. It should be noted that the vapour diffusion is closely connected with the mechanism of phase changes maintaining the condition of quasi-saturation. However, the contribution of the latent heat to the stability is shown to be less important in this problem. In § 5 physical explanations of these phenomena are given.

An experiment to test the mathematical analysis has been carried out. The composite fluid used mainly in the experiment consisted of air, water vapour and water droplets. The droplet suspensions were produced by injecting cigarette smoke into the layer of air saturated with water vapour to provide nuclei. In the

experiment the state of the fluid system was unsteady owing to sedimentation of droplets. However we think, as the qualitative arguments in § 8 confirm, that the speed of falling was slow enough for the system to be regarded as quasi-steady. This variation of the basic state of the system corresponds to a movement of the 'state point' in a certain phase plane (the R, S plane in later sections). Thus comparison is possible between the experiment and the theory, and qualitative agreement has been obtained. It is shown further that the observed difference in behaviour between the composite fluid mentioned above and that formed using alcohol instead of water is consistent with the theoretical analysis.

The mathematical analysis is performed in §§ 2–4 and summarized in § 5. In § 6 the experimental apparatus is illustrated and the observed phenomena are described in § 7. In the final selection the experimental observations are compared with the theoretical results.

2. Formulation of the problem

We consider a fluid which is composed of a nearly saturated vapour (superscript v), an inert carrier gas (superscript i) and small liquid droplets (superscript d). The governing equations are as follows.

Continuity equations

$$\nabla . \mathbf{v} = 0, \tag{1}$$

$$\frac{D}{Dt}\rho^v = \eta + D_m \nabla^2 \rho^v, \quad \frac{D}{Dt} r = -\frac{1+r}{\rho^g}\eta, \tag{2), (3}$$

where $\mathbf{v}$ is the mean velocity of the three components, η the local mass production rate of vapour, ρ^v and ρ^g ($\equiv \rho^v + \rho^i$) the vapour density and the total gas density respectively, r the droplet mass fraction, defined as ρ^d/ρ^g (ρ^d = mass of droplets per unit volume of the fluid), and D_m the mutual mass diffusivity of the two gaseous constituents. The operator D/Dt denotes substantial differentiation following the mean motion.

Equation of motion

$$\rho D\mathbf{v}/Dt = -\nabla p + \mu \nabla^2 \mathbf{v} + \rho \mathbf{g}, \tag{4}$$

where ρ is the total density, p the total pressure, μ an effective dynamic viscosity of the fluid and $\mathbf{g}$ the acceleration due to gravity.

Equations of energy

$$\rho^g C_p^g DT/Dt = k_T \nabla^2 T + h, \tag{5}$$

$$\rho^d C^d DT^d/Dt = -h - \lambda\eta, \tag{6}$$

where T ($\equiv T^g = T^i = T^v$) and T^d are the temperatures of the gas and the droplets respectively, C_p^g the specific heat of the gas phase at constant pressure, C^d the specific heat of the droplets, k_T the thermal conductivity, λ the latent heat per unit mass and h the heat transfer rate from the droplets to the gas. All physical quantities such as μ, k, D_m, C_p^g and C^p are assumed constant.

Equation of state

$$p^i = R^i \rho^i T, \quad p^v = R^v \rho^v T, \quad p^i + p^v = p, \tag{7}$$

where the p's and R's are partial pressures and gas constants respectively. The total pressure p is assumed constant except in (4).

The vapour production rate and heat transfer rate are given by

$$\eta = \{\rho_s(T^d) - \rho^v\}/\tau_v, \tag{8}$$

$$h = \rho^g C_p^g (T^d - T)/\tau_T, \tag{9}$$

where τ_v and τ_T are characteristic times for the respective relaxation processes and $\rho_s(T^d)$ is the density at the saturation vapour pressure at T^d. When $\rho_s \ll \rho$, i.e. when T^d is far below the boiling point, ρ_s is written in the linear approximation as

$$\rho_s(T) = \rho_s(T_*) + \phi_*(T - T_*), \tag{10}$$

where $\phi_* \equiv d\rho_s(T_*)/dT$. In this equation and below asterisks denote averages over the layer.

From the definition of r and (7), we have

$$\left.\begin{aligned} \rho &\equiv \rho^g + \rho^d = \rho^g(1+r), \\ \rho^g &\equiv \rho^i + \rho^v = p/R^iT - \gamma\rho^v, \end{aligned}\right\} \tag{11}$$

where $\gamma = R^v/R^i - 1 = M^i/M^v - 1$ with M^i and M^v the molecular weights of the inert gas and the vapour respectively. The total density is written in the linear approximation as

$$\left.\begin{aligned} \rho &= \rho_*\left\{1 - \hat{\alpha}(T - T_*) + \frac{1}{1+r_*}(r - r_*)\right\}, \\ \hat{\alpha} &= \alpha^g + \frac{\gamma\phi_*}{\rho_*^g}, \quad \alpha^g = \frac{1}{T_*}\left(1 + \gamma\frac{\rho_{s*}}{\rho_*^g}\right), \end{aligned}\right\} \tag{12}$$

where we have used the definitions (11), equations of state (7) and the approximate relation $p^v \approx p_s(T)$. The quantity $\hat{\alpha}$ is an effective thermal expansion coefficient.

Governing equations for a gas carrying small non-volatile particles (i.e. a dusty gas) are obtained by letting $\eta = 0$ and omitting (2) and the quantities associated with the vapour.

3. Perturbation equations and simplification

The stability of a horizontal layer of the three-component fluid of thickness d subjected to both a temperature gradient $-a$ and a gradient of particle mass fraction $-b$ is studied. We introduce a Cartesian co-ordinate system in which the x and y axes lie on the horizontal lower boundary and the z axis is vertically upwards. The basic stationary state, whose stability is under consideration, is defined by the equations

$$\mathbf{v} = 0, \quad T = T^d = T_0(z) \equiv T_* - a(z - \tfrac{1}{2}d), \tag{13a,b}$$

$$\rho^v = \rho_s(T_0), \quad r = r_0(z) \equiv r_* - b(z - \tfrac{1}{2}d), \tag{13c,d}$$

$$\rho = \rho_0 = \rho_*\{1 + [\hat{\alpha}a - b/(1+r_*)](z - \tfrac{1}{2}d)\}, \tag{13e}$$

$$p = p_0 = -g\int^z \rho_0\, dz, \quad \eta = h = 0. \tag{13f,g}$$

This is an exact solution of (1)–(6). The basic distribution r_0 of the droplet

fraction r cannot be determined uniquely from the governing equations. For the sake of simplicity, we confine ourselves to the above linear distribution.

We superimpose small perturbations on the basic state as follows:

$$\left.\begin{aligned} &\mathbf{v} = (u, v, w), \quad T = T_0 + T_1, \quad T^d = T_0 + T_1^d, \\ &\rho = \rho_0 + \rho_1, \quad \rho^v = \rho_s(T_0) + \rho_1^v, \quad r = r_0 + r_1, \end{aligned}\right\} \tag{14}$$

where perturbation terms are indicated by a suffix 1. The linearized equations for the perturbations are

$$\nabla . \mathbf{v} = 0, \tag{15}$$

$$\partial \rho_1^v / \partial t - a\phi_* w = \eta + D_m \nabla^2 \rho_1^v, \tag{16}$$

$$\frac{\partial r_1}{\partial t} - bw = -\frac{1 + r_*}{\rho_*^g} \eta, \tag{17}$$

$$\rho_* \, \partial \mathbf{v} / \partial t = -\nabla p_1 + \mu \nabla^2 \mathbf{v} + \rho_1 \mathbf{g}, \tag{18}$$

$$\rho_*^g C_p^g (\partial T_1 / \partial t - aw) = k_T \nabla^2 T_1 + h, \tag{19}$$

$$\rho_*^d C^d (\partial T_1^d / \partial t - aw) = -h - \lambda \eta, \tag{20}$$

where, by using (8)–(12),

$$\eta = (\phi_* T_1^d - \rho_1^v)/\tau_v, \quad h = \rho_*^g C_p^g (T_1^d - T_1)/\tau_T, \tag{21}$$

$$\rho_1 = \rho_* [-\hat{\alpha} T_1 + (1 + r_*)^{-1} r_1]. \tag{22}$$

To simplify these equations further, we introduce a new variable T', defined by

$$\rho_1^v = \phi_* (T_1 + T'). \tag{23}$$

T' is a measure of the departure from the equilibrium condition. As stated in § 1, the relaxation times τ_v and τ_T are assumed to be small enough to satisfy the inequalities

$$\frac{\rho_*^g C_p^g}{\rho_*^d C^d} \frac{1}{\tau_T} \gg \frac{1}{\tau_c}, \quad \frac{\lambda \phi_*}{\rho_*^d C^d} \frac{1}{\tau_v} \gg \frac{1}{\tau_c},$$

where τ_c is a characteristic time of the convective motion of the perturbation. Then we obtain $h \approx -\lambda \eta$ from (20), which means that the energy lost by each droplet owing to evaporation is immediately compensated for by heat transfer from the surrounding gas. Using this relation and (23) we obtain from (21)

$$h = \lambda \phi_* T'/\tau_0, \quad \eta = -\phi_* T'/\tau_0, \tag{24}$$

where

$$\tau_0 = \tau_v + \Phi \tau_T, \quad \Phi = \lambda \phi_* / \rho_*^g C_p^g .\dagger$$

Substituting (23) into (16) and using (19) and (24), we have

$$\partial T'/\partial t = -\kappa^g \nabla^2 T_1 + D_m \nabla^2 (T_1 + T') - (1 + \Phi) T'/\tau_0, \tag{25}$$

where $\kappa^g = k_T / \rho_*^g C_p^g$. Since τ_0 is much smaller than both τ_c and the diffusion time d^2/D_m, we obtain the approximate relation

$$(1 + \Phi) T'/\tau_0 = (D_m - \kappa^g) \nabla^2 T_1 \tag{25a}$$

† The quantity Φ is the ratio of the heat required for evaporation when the temperature is raised by 1 °C to the heat capacity of the gas phase; hence it is a measure of the effectiveness of the latent heat.

from (25). Then the vapour production rate η reduces to

$$\eta = -\phi_*(1+\Phi)^{-1}(D_m-\kappa^g)\nabla^2 T_1. \tag{26}$$

We infer from (26) that the relative magnitude of the two diffusion coefficients D_m and κ^g is important in the problem under consideration.

The energy equation, obtained by adding (19) to (20), reduces to

$$\overline{\rho C}(\partial T_1/\partial t - aw) = k_T \nabla^2 T_1 - \lambda\eta, \tag{27}$$

where $\overline{\rho C} = \rho_*^g C_p^g + \rho_*^d C^d$ and we have neglected the term involving $\partial T'/\partial t$ since $T'/T_1 = O(\tau_0(d^2/D_m)^{-1})$ from (25*a*).

Lastly,

$$\nabla^2\{z \text{ component of (18)}\} - \partial\{\nabla\,.\,(18)\}/\partial z,$$

together with (15), gives

$$\rho_* \partial(\nabla^2 w)/\partial t = \mu\nabla^2\nabla^2 w - g\Delta_2\rho_1, \tag{28}$$

where

$$\left.\begin{aligned} \rho_1 &= \rho_*[-\hat{\alpha}T_1 + (1+r_*)^{-1} r_1], \\ \Delta_2 &= \partial^2/\partial x^2 + \partial^2/\partial y^2. \end{aligned}\right\} \tag{29}$$

Eliminating η from (17) and (27) and using (26) and ρ_1 from (28) by using (29), we have the following reduced set of equations for w, T_1 and r_1:

$$\partial(\nabla^2 w)/\partial t = \hat{\nu}\nabla^2\nabla^2 w + g\Delta^2[\hat{\alpha}T_1 - (1+r_*)^{-1} r_1], \tag{30a}$$

$$\partial T_1/\partial t = aw + \hat{\kappa}\nabla^2 T_1, \tag{30b}$$

$$\partial r_1/\partial t = bw + \beta\nabla^2 T_1, \tag{30c}$$

where

$$\hat{\nu} = \mu/\rho_* = \nu^g/(1+r_*), \quad \nu^g = \mu/\rho_*^g, \tag{31a}$$

$$\hat{\kappa} = \kappa^g\left(1 + \frac{\Phi}{1+\Phi}(L-1)\right)\frac{\rho_*^g C_p^g}{\overline{\rho C}}, \tag{31b}$$

$$\beta = (D_m - \kappa^g)\frac{\phi_*}{1+\Phi}\frac{1+r_*}{\rho_*^g}, \tag{31c}$$

$$L = D_m/\kappa^g \quad \text{(Lewis number)}. \tag{31d}$$

Here it may be interesting to compare equations (30) with those for the double-diffusive system (see Turner 1973) mentioned in § 1. Both systems consist of three equations for three variables: the vertical velocity, the first diffusing property (temperature) and the second diffusing property (the droplet mass fraction r in the present case, the salinity in the thermohaline case). The main difference lies in the equations for the second properties. In the thermohaline case the rate of change of salinity following the motion is related to the diffusion of salt, while in the present case the rate of change of the droplet-fraction perturbation r_1 is related to the term $\beta\nabla^2 T$ (the vapour condensation rate), the sign of β depending on the relative size of D_m and κ^g, and the diffusion of r is neglected. In appendix A the effect of the diffusivity of r is discussed. Equations (30) also bear some resemblance to those given by Schechter *et al.* (1972). If the coefficient D in

equation (1) of their paper is neglected and the coefficient $D'N_1^* N_2^*$ is replaced by β, the system of equations is formally identical to (30).†

We normalize length and time by using d and $d^2/\hat{\kappa}$ respectively, retain the same notation for the normalized quantities and look for solutions of the form

$$(T_1, w, r_1) = \left(\Theta(z), \frac{\hat{\kappa}}{ad^2} W(z), \frac{b}{a}\Psi(z)\right) \exp\left[\sigma t + i(k_x x + k_y y)\right]. \tag{32}$$

Substituting these into (30), we obtain the following set of equations:

$$(D^2 - P^{-1}\sigma) D^2 W = Rk^2(\Theta - S\Psi), \tag{33a}$$

$$D^2\Theta - \sigma\Theta = -W, \quad KD^2\Theta - \sigma\Psi = -W, \tag{33b,c}$$

where

$$D^2 = d^2/dz^2 - k^2, \quad k^2 = k_x^2 + k_y^2, \tag{34a}$$

$$K = Q/S = \beta a/\hat{\kappa} b, \tag{34b}$$

$$P = \hat{\nu}/\hat{\kappa} \quad \text{(modified Prandtl number)}, \tag{34c}$$

$$Q = \beta/\hat{\kappa}\hat{\alpha}(1 + r_*) \quad \text{(parameter characterizing strength of vapour condensation rate)}, \tag{34d}$$

$$R = g\hat{\alpha}ad^4/\hat{\kappa}\hat{\nu} \quad \text{(modified Rayleigh number)}, \tag{34e}$$

$$S = b/a\hat{\alpha}(1 + r_*) \quad \text{(ratio of the droplet density gradient to the gas density gradient)}. \tag{34f}$$

Elimination of W and Ψ from (33) yields

$$D^6\Theta - \left(1 + \frac{1}{P}\right)\sigma D^4\Theta + \left\{\frac{\sigma^2}{P} + (1 - K)SR\frac{k^2}{\sigma}\right\} D^2\Theta + (1 - S)Rk^2\Theta = 0. \tag{35}$$

We assume the following boundary conditions at $z = 0$ and 1:

$$\Theta = 0, \quad W = 0, \tag{36a,b}$$

$$\left.\begin{aligned} &W'' = 0 \quad \text{(for a free wall)} \\ \text{or} \quad &W' = 0 \quad \text{(for a rigid wall)}, \end{aligned}\right\} \tag{36c}$$

where a prime denotes a derivative with respect to z. Condition (36a) is obtained from the condition of fixed wall temperature, which is valid if the walls have high thermal conductivity and large heat capacity. The conditions for $W(z)$ are transformed into those for Θ by using (33b).

Equation (35) and the boundary conditions (36) constitute an eigenvalue problem in which σ can take a complex value and the sign of $\mathrm{Re}\,(\sigma)$ determines the stability of the system.

Note that the modified Rayleigh number R can be expressed as

$$\left.\begin{aligned} &R = R^g F \frac{\overline{\rho C}}{\rho_*^g C_p^g}(1 + r_*), \\ \text{with} \quad &R^g = \frac{g\alpha^g a d^4}{\kappa^g \nu^g}, \quad F = \frac{1 + \gamma\phi/\alpha^g\rho_*^g}{1 + (L - 1)\,\Phi/(1 + \Phi)}. \end{aligned}\right\} \tag{37}$$

† However, in their system the basic gradient of the second property (N_1 in their notation) is determined from a given temperature distribution, while the gradient of r is arbitrary in our problem.

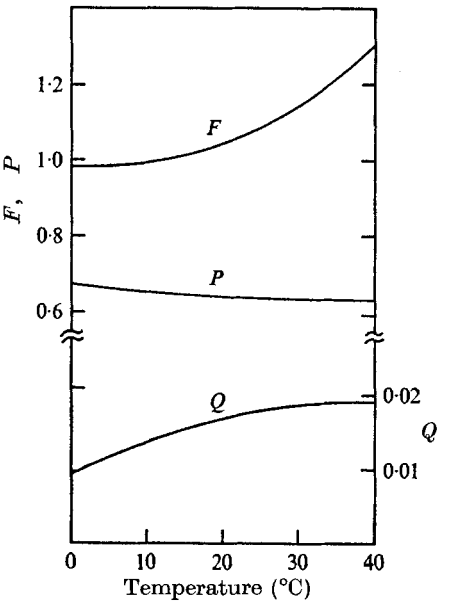

FIGURE 1. F, P and Q *vs.* temperature.

Figure 1 shows the variation with temperature of P, Q and F for air saturated with water vapour, where $r_* \ll 1$. In most practical cases Q is less than unity: for example, $Q \sim 0{\cdot}01$ for a mixture of air and saturated vapour at 10 °C, $Q = 0$ for a dusty gas and $Q < 0$ for a mixture of air and a saturated common organic material, such as alcohol. Hence we confine ourselves to the case $Q < 1$ below.

4. Stability analysis

4.1. *Solution for free walls*

Separate analyses are given for different regions of the S, R plane. However the results are first shown schematically in figure 2.

The case $K = 1$ ($S = Q$). It may be interesting to examine first the case $K = 1$, in which equation (35) reduces to that for the classical problem of thermal convection if the parameter $(1 - S)\,R$ is considered as an effective Rayleigh number. Thus the critical condition for the onset of instability is

$$(1 - S)\,R = R_0, \tag{38†}$$

where R_0 is the critical Rayleigh number $\frac{27}{4}\pi^4$ in the classical problem. The eigenvalue σ is real in this case and steady convection appears in the marginal state.

Since the effect of latent heat is represented by the factor $(L - 1)\,\Phi/(1 + \Phi)$ in (37), the critical value of R^g, the Rayleigh number of the gas phase, increases or decreases according as the Lewis number L is larger or smaller than unity, i.e. $D_m \gtrless \kappa^g$. Therefore the latent heat does not always lead to destabilization if the diffusion phenomena are important.

† The relation (38) shows that the presence of the droplet distribution, represented by the parameter S, increases the critical value of R for $1 > S > 0$ (stabilizing) but decreases it for $S < 0$ (destabilizing).

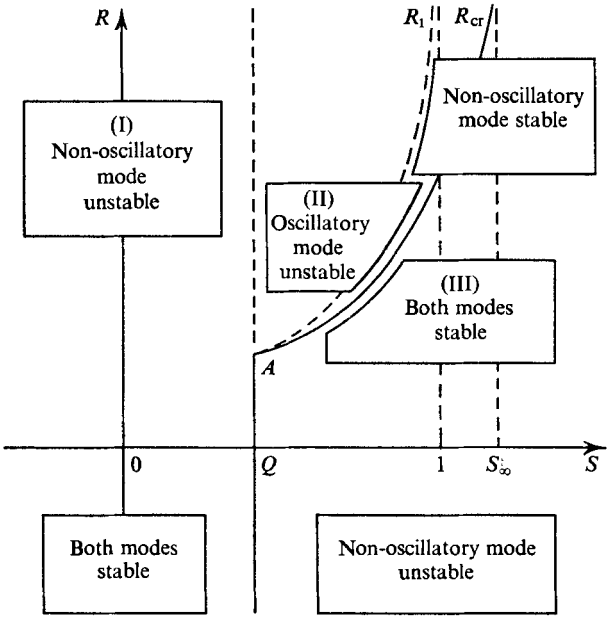

FIGURE 2. Stability characteristics in the S, R plane for the free-wall case. On the line $S = Q$, the non-oscillatory mode is unstable above the point A ($R_A = \frac{27}{4}\pi^4(1-Q)$) and stable below it. $S_\infty = (1-Q+P)/P$. The situation is the same in the rigid-wall case.

The case $K \neq 1$ ($S \neq Q$), $R > 0$. The solution of (35) satisfying the boundary conditions (36*a*, *b*) and the free-wall condition (36*c*) is given by

$$\Theta = \sin n\pi z, \tag{39}$$

where n is an integer. Substitution of this into (35) leads to a cubic equation for σ:

$$f(\sigma) \equiv N^2\sigma^3 + (1+P)N^4\sigma^2 + P[N^6 - (1-S)Rk^2]\sigma + (1-K)PSRk^2N^2 = 0, \tag{40}$$

where $N^2 = n^2\pi^2 + k^2$. This equation determines the eigenvalue σ as a function of k and n with four given parameters, P, R, S and K. The eigenvalue σ is complex in general and is written as $\sigma = \sigma_r + i\sigma_i$ (σ_r and σ_i are real).

(*a*) *The case* $S < Q$ (*region* I). Since $f(0)$ is negative and the coefficient of σ^3 is positive, (40) has at least one real positive root. If the remaining two roots are real, they must be negative since $f(0) < 0$ and the inflexion point of the cubic curve occurs at negative σ. Even if (40) has complex roots, we can show that their real part should be negative (see appendix B). Thus we can say that there is only one root with $\sigma_r > 0$, and that its imaginary part is zero. Hence there is an unstable mode irrespective of the Rayleigh number R, and thus the critical Rayleigh number is zero,† and in the unstable mode the perturbation grows exponentially without oscillation. The growth rate σ depends on R.

In a dusty gas this instability sets in for $S < 0$ since $Q = 0$. On the other hand, in a fluid mixture with $Q > 0$ it sets in even for positive S irrespective of the Rayleigh number R if $S < Q$, although positive S (droplets more abundant in the

† If droplet diffusion is present, the critical Rayleigh number becomes positive (non-zero) (see appendix A).

lower part of the layer) is thought to be a stabilizing factor. A similar example is seen in the thermohaline system (Baines & Gill 1969; Turner 1973), however the critical Rayleigh number is greater than R_0.

(*b*) *The case* $S > Q$ (*regions* II *and* III). Here, in order to see the dependence of stability on R, we define a quantity $R_1 = N^6 k^{-2}/(1-S)$. All the coefficients in (40) are positive in the case $S > 1$ and in the case $S < 1$, $R < R_1$. Hence (40) has at least one negative root, and if the remaining two roots are real, they should be negative. Thus the non-oscillatory mode ($\sigma_i = 0$), if it exists, is stable in these cases.

However, in some region of the S, R plane, (40) has complex roots, yielding an oscillatory mode. In order to examine the marginal state of this mode, we set $\sigma = i\sigma_i\,(\sigma_r = 0)$ and substitute this into (40). Then we find from its real and imaginary parts

$$\sigma_i^2 = (S-Q)\frac{P}{1+P},\quad R\frac{k^2}{N^2}, \tag{41}$$

$$R = \frac{N^6}{k^2}\Big/\left(1-\frac{Q+PS}{1+P}\right) = R_m, \quad \text{say.} \tag{42}$$

The value of R_m becomes infinite at $S = S_\infty \equiv (1+P-Q)/P\,(>1)$. It is easy to show that $R_m < R_1$ if $S < 1$, hence the oscillatory mode (or travelling wave) is more unstable than the non-oscillatory mode discussed above. The oscillatory mode also grows in the case $1 < S < S_\infty$. Therefore the transition from stability to instability occurs via a state of oscillation when $Q < S < S_\infty$, and the critical Rayleigh number $R_{\rm cr}$ (the boundary between regions II and III) is found by replacing the factor N^6/k^2 in (42) by its minimum value $\frac{27}{4}\pi^4$.

As may be inferred from the definition of S in (34*f*) and ρ_0 in (13*e*), the total density decreases upwards if $S > 1$. Thus the above result states that the system can become unstable even when the total density distribution is gravitationally stable. It may be said from (41) that the oscillation in the system is caused by two factors: the droplet distribution, represented by S, and the phase transition, represented by Q.†

Figure 3 is an S, R diagram for a fluid with $P = 0{\cdot}65$ and $Q = 0{\cdot}01$, where lines of constant $\sigma_r^{(m)}$ (the maximum σ_r for varying k) and of constant σ_i for $\sigma_r = \sigma_r^{(m)}$ are shown. The critical Rayleigh number at A (say R_A) is $\frac{27}{4}\pi^4/(1-Q) \sim 664$. The broken line BAC shows the lower limit of R for complex roots to exist. Note that the value of r_* does not essentially affect the stability characteristics if $r_* \ll 1$, since it always appears in the combination $1+r_*$.

The case $R \leqslant 0$. An analysis similar to those above is also possible here. The case $R < 0$ physically corresponds to heating from above ($a < 0$), a situation which is gravitationally stable in a simple fluid. It can be shown in this case that the system is stable or unstable depending on whether $S-Q$ is negative or positive. Note that, when the sign of a changes, the sign of S also changes for the same b. The instability may be attributed to the droplet distribution being gravitationally unstable.

† For large k^2 the term $SP(1+P)^{-1}Rk^2/N^2$ appearing on the right-hand side of (41) corresponds to $\omega_{BV}^2/(1+P)$ in dimensional units, where ω_{BV} is the Brunt–Väisälä frequency for a stable droplet distribution, defined by $(-g\rho^{*-1}d\rho^d/dz)^{\frac{1}{2}}$.

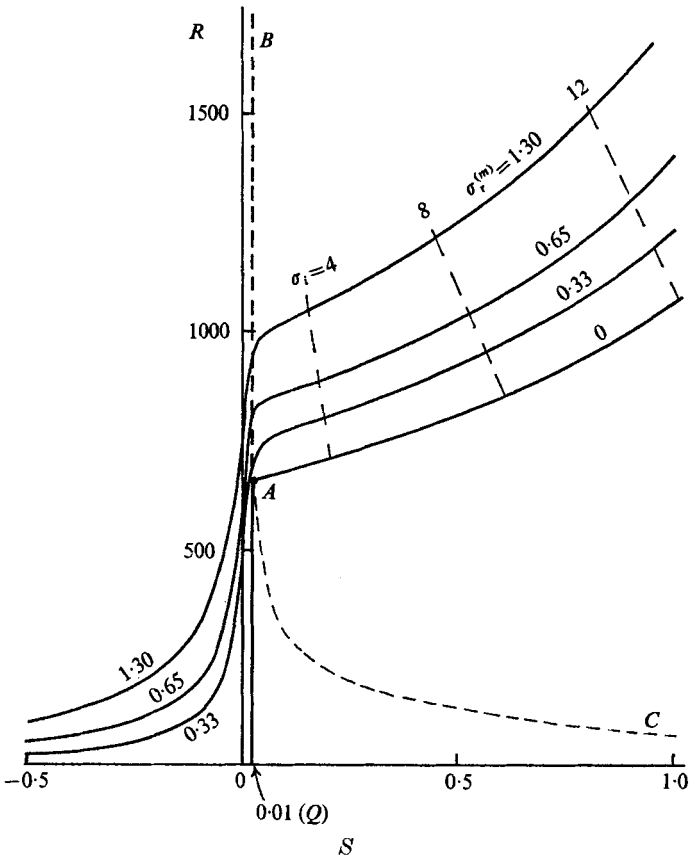

FIGURE 3. Lines of constant growth rate $\sigma_r^{(m)}$ (solid lines) and constant frequency σ_i (broken lines) for $P = 0{\cdot}65$ and $Q = 0{\cdot}01$ for the free-wall case. $S_\infty = 2{\cdot}52$. Complex roots do not exist below the line BAC.

The case $R = 0$ ($a = 0$) must be dealt with by going back to (30). It is found, by setting $T_1 = 0$, that the system is stable or unstable depending on whether b is positive or negative.

4.2. *Solution for rigid walls*

When $K = 1$ ($S = Q$), the situation is the same as that in the free-wall case. The critical Rayleigh number is given by (38), where R_0 is here 1707·8.

When $K \neq 1$, a general solution of the sixth-order linear equation (35) can be constructed in the form

$$\Theta = \sum_{i=0}^{5} A_i f_i(z), \tag{43}$$

where the A_i are six constants and the f_i are six mutually independent functions satisfying (35). According to the method of Sparrow, Goldstein & Jonsson (1964), the f_i may be expressed as

$$f_i(z) = \sum_{n=0}^{\infty} a_{i,n} z^n \quad (i = 0, 1, \ldots, 5). \tag{44}$$

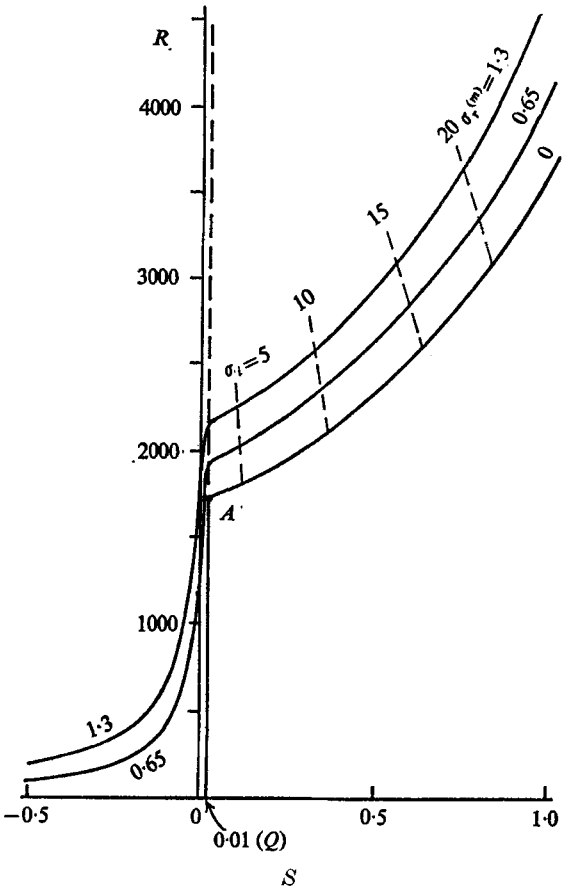

FIGURE 4. Lines of constant growth rate $\sigma_r^{(m)}$ (solid lines) and constant frequency σ_i (broken lines) for $P = 0{\cdot}65$ and $Q = 0{\cdot}01$ for the rigid-wall case. $R_A = 1708/(1-Q) = 1725$.

Without loss of generality we can put $a_{i,n} = \delta_{in}\,(i = 0, \ldots, 5)$, then the other coefficients can be determined uniquely from (35). The constants $A_i\,(i = 0, \ldots, 5)$ are to be determined from boundary conditions (36*a*, *b*) and the rigid-wall condition (36*c*). The requirement of a non-vanishing solution leads to a characteristic equation for σ and k including four parameters, P, R, S and K (or Q), which can be solved numerically.

It may be shown that the real part of σ has a maximum value $\sigma_r^{(m)}$ when k is varied for fixed R and S (and also for fixed P and Q, which are material constants except for the unimportant factor $1 + r_*$ in Q). The neutral curve ($\sigma_r^{(m)} = 0$) and equal-$\sigma_r^{(m)}$ and equal-σ_i curves are presented in figure 4 for the same fluid as in figure 3. The critical Rayleigh number R_A at A is $1708/(1-Q) = 1725$. In both figures 3 and 4 the frequency σ_i, roughly speaking, depends on S and increases with it.

Figure 5 shows the growth rate σ_r for $P = 0{\cdot}65$, $Q = 0{\cdot}01$ and $S = 0$ (region I) as a function of R and k. The maximum of σ_r occurs at $k = 3$–4. The relation between this maximum $\sigma_r^{(m)}$ and R is shown in figure 6. The value of $\sigma_r^{(m)}$ exceeds one at

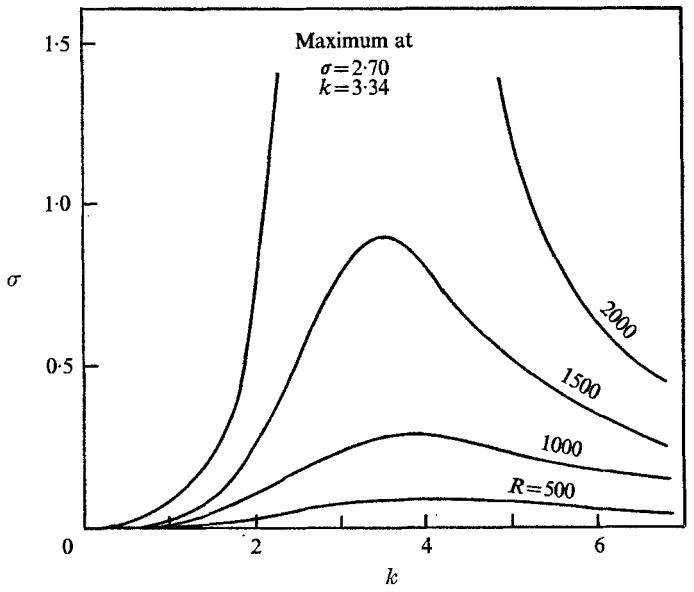

FIGURE 5. Growth rate of the non-oscillatory mode for the rigid-wall case as a function of k for various R, with $P = 0{\cdot}65$, $Q = 0{\cdot}01$ and $S = 0$.

$R \approx 1500$ and increases rapidly for larger R.† Because of the normalization of the time mentioned in §3, the condition $\sigma_r = 1$ means that the characteristic time of growth is equal to the time for heat to diffuse across the layer, i.e. $d^2/\hat{\kappa}$.

5. Summary of the analysis

The thermal instability of a three-component fluid has been discussed under the assumptions that the fluid satisfies a Boussinesq-like approximation, that the droplets are sufficiently small and dense, that the Brownian motion and sedimentation of droplets may be neglected, that the characteristic times of thermodynamic relaxations are sufficiently small, i.e. the vapour is nearly saturated, and that the inert gas contributes the main fraction of the mass. The dynamical behaviour of such a fluid is governed by the set of equations (30) or (33) and characterized by the non-dimensional parameters P, Q (or K), R and S, defined in (34).

In the free-wall case, an oscillatory mode appears when R is higher than a certain critical value for $Q < S < S_\infty$, the layer is completely stabilized for $S > S_\infty$, and the non-oscillatory mode grows for $S < Q$. Similar results are obtained in the rigid-wall case. The stability characteristics depend strongly on the difference $D_m - \kappa^g$. For example, when $Q (\propto D_m - \kappa^g) > 0$, the system is completely unstable for $0 < S < Q$, though a positive S is thought to be a stabilizing factor.

The mechanism of this absolute instability may need some explanation. When $S < Q\,(K > 1)$, the term $KD^2\Theta$ in (33c), which is associated with vapour condensation, is more dominant than the term $D^2\Theta$ in (33b), which represents heat

† A similar curve is obtained for the free-wall case, where $\sigma_r > 1$ for $R > 700$.

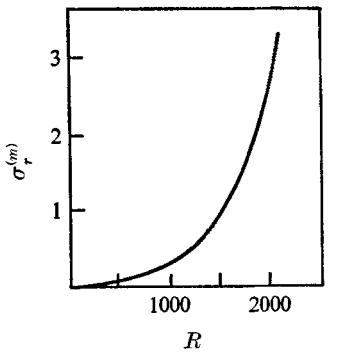

FIGURE 6. Curve of maximum growth rate $\sigma_r^{(m)}$ *vs.* R, which corresponds to the peaks of the curves in figure 5.

diffusion. Now consider a parcel of fluid in the layer with a higher temperature than its surroundings. In this parcel vapour is more abundant than in its surroundings. Therefore both temperature (heat) and vapour diffuse outwards from the parcel. However, owing to the inequality $D_m > \kappa^q$ $(Q > 0)$, vapour diffuses more rapidly than heat (in a qualitative sense), the vapour diffusion being followed by immediate vapour production from liquid droplets in the parcel. Thus the total mass of droplets in the parcel decreases rapidly, while cooling by heat diffusion is comparatively slow. As a consequence the parcel becomes lighter under certain conditions than its surroundings. In this way, the instability sets in. However the onset of this instability is confined to the case $S < Q$. For larger S the growth of perturbations may be inhibited by the stable distribution of droplets. This instability might be called 'evaporation instability' or 'condensation instability'.

The existence of latent heat has no decisive effect on instability. The reason is that the latent heat of the vapour causes increases in both an effective heat capacity and an effective heat conductivity (through vapour diffusion) of the composite fluid, hence the two opposing effects of the latent heat on the effective thermometric conductivity $\hat{\kappa}$ offset each other, giving only a small correction.

The physical picture of the oscillatory mode appearing in regions II and III resembles to some extent that of thermohaline convection, described fully by Veronis (1965), if the droplet fraction is replaced by salinity.

6. Experimental apparatus and methods

An experiment to test the above results has been carried out. Figure 7 shows schematically the apparatus, in which a horizontal layer of composite fluid (a cloud) was formed with an imposed temperature gradient. Two square vessels C and D of acrylic resin with sides of length 13 cm contained pure hot and cold water respectively, so that the convection layer A was bounded by a surface of the hot water and the under surface of D, and was considered to be saturated with water vapour. An aluminium plate B was placed at a depth of 1 mm below the surface in order to check convective motion in the hot water. It was covered with black cloth for the purpose of obtaining a better view of the motions in A

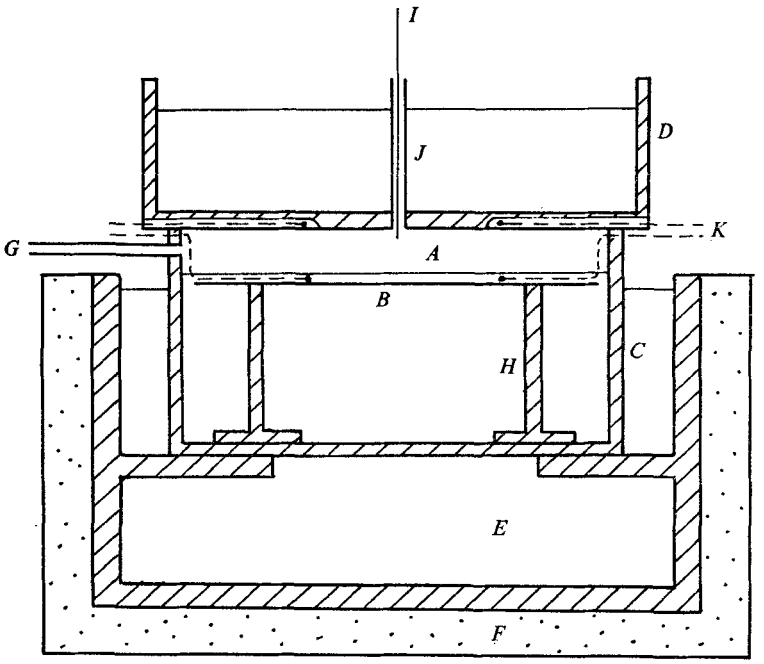

FIGURE 7. Side view of the convection chamber. A, convection layer; B, aluminium plate covered with black cloth; C, hot-water vessel of acrylic resin; D, cold-water vessel of acrylic resin; E, hot bath; F, styrofoam; G, pipe for smoke injection; H, support of aluminium plate; I, needle for measuring thickness of A; J, tube for needle I; K, thermocouples.

from above. The vessel C was put in a hot-water bath E covered with styrofoam F, which was placed on a base with equipment for levelling. The difference between the temperatures of the water in C and D was changed between 5 and 20 °C such that the higher temperature did not exceed 50 °C. In order to keep the upper boundary of A wet and also to assure a clear top view of the motion, its surface was sprayed with defrosting liquid for car windows.

The droplet suspension (cloud) was produced by injecting cigarette smoke into A through a pipe G to provide nuclei. The smoke particles had the advantage of acting as flow tracers as well. We observed the development of the layer of composite fluid after a finite-time injection for about one second. The mean pressure in A was always kept at atmospheric since there was an opening between C and D; this was narrow enough to have little effect on the convective motion in A. For the sake of comparison convective motion in dry air has been observed, using (non-volatile) glycerin instead of hot water.

The thickness d of A was varied between 8 and 13 mm and measured to within an error of 0·1 mm by inserting a thin needle I through the pipe J. The temperature difference ΔT between the upper and lower boundaries was measured by two copper–constantan thermocouples K connected in series. The temperature T_L of the lower boundary was sometimes measured by inserting a semiconductor thermometer. From the measured values of d, ΔT and the mean temperature T_* ($= T_L + \frac{1}{2}\Delta T$) we can calculate the Rayleigh number R defined by (37), where

the factors $\overline{\rho C}/\rho_*^g C_p^g$ and $1 + r_*$ are put equal to 1 since $r_* \ll 1$ in our experiment. The error in the value of R comes from those in d, ΔT and T_*, and is about 5 %.

Side-wall effects have not been examined critically, but the observed flow patterns were not greatly affected by the side walls. Though this experimental system is quite simple and roughly constructed, it is sufficient for examining the qualitative nature of the motion.

Photographs and recordings on video tape were taken from above. The side view of the motion could be seen more clearly in a smaller and simpler convection chamber with a horizontal cross-section 5 × 7 cm, and was photographed together with the top view.

7. Experimental results

7.1. *Observed phenomena*

Soon after the smoke injection droplets began to grow in size and fall down quite slowly, hence a density gradient due to the non-uniform distribution of the droplets was formed besides the given temperature gradient. The natural development of the droplet distribution due to the sedimentation tended to make the droplet gradient parameter b positive and increase gradually. Correspondingly the parameter S, which was positive, increased slowly. Thus the 'state point' in the R, S plane moved to the right. At the bottom of the layer the droplets dissolved into the hot water and the droplet density decreased, therefore after a while its gradient also decreased and the state point in the R, S plane turned back again to the left. During this process motions corresponding to different regions in the S, R plane appeared successively. Thus, observation of the phenomena in the layer A will offer a test of the theoretical result shown in figure 2. During the sequence of several phases of the system in each experimental run described below, the Rayleigh number R is considered to remain almost constant. We confine ourselves to the phenomena after the smoke injection, for any motion before that is hard to observe and does not seem to affect the subsequent phenomena. The sequences of phases observed with different Rayleigh numbers are summarized diagrammatically in figure 8.

The first phase observed was a flow induced by the smoke injection (the *initial* phase). The appearance of this phase depended on how the smoke was injected and not on the Rayleigh number. It lasted for a few seconds and the next phase followed immediately. A typical example is shown in figure 9(*a*) (plate 1).

The phase following the *initial* phase was different for different ranges of R. If $R < R_c \approx 1800$, the fluid became still with only the droplet sedimentation proceeding quite slowly (this phase was named the *static* phase). On the other hand, if $R \gtrsim R_c$ a convective motion with cells appeared (the *cellular* phase). An example of the *cellular* phase is shown in figure 9(*b*) (plate 1). The lifetime of this phase increased with R, and became half a minute at $R \sim 5000$. For R slightly larger than R_c, the *cellular* phase was followed by the *static* phase mentioned above. If R was much larger than R_c, each cell boundary in the *cellular* phase drifted randomly, and following this phase a new motion involving travelling waves appeared (this is named the *wave* phase). During the motion the cloud of droplets

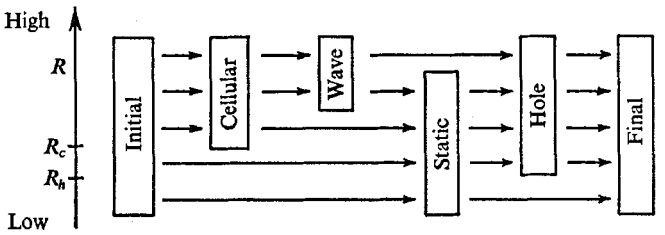

FIGURE 8

was falling downwards, and the upper surface of the cloud layer performed wavy motions similar to water waves. An example of the *wave* phase is shown in figure 9(*c*) (plate 1). The duration of the *wave* phase also increased with R. So long as R was only moderately larger than R_c, the *wave* phase decayed after a time and was followed by the *static* phase.

The phases after the *static* phase were as follows. If $R < R_h \approx 1400$, the *static* phase lasted for the order of a minute and the cloud disappeared by sedimentation, no change being observed until another smoke injection was made (this last phase is named the *final* phase). If $R \gtrsim R_h$, several circular holes appeared spontaneously when the calm cloud layer settled into a thin layer just above the bottom (see figures 9*d* and 10*a*). The motion, though quite slow, was seen to be downwards at the hole centre and upwards at the periphery, so that the part of the cloud in the central part was swept to the periphery. After a while the whole area was covered with such holes, and they then rearranged themselves into a regular and stationary honeycomb pattern. Examples of this phase (the *hole* phase) are shown in figures 9(*e*) and (*f*) (plate 2). The *hole* phase gradually faded through the diffusion of the cloud (also named the *final* phase); for relatively larger R, the remaining faint cloud showed cellular convective motion (figure 9*h*), while for smaller R, the layer became transparent without any visible motion as in the case $R < R_h$ (figure 9*g*, plate 2).

When R was sufficiently larger than R_c, the fluid layer showed the *cellular* and *wave* phases in series, but the *static* phase did not follow the *wave* phase. At a later stage of the *wave* phase the motion became turbulent and sometimes isolated holes like those in the initial stage of the *hole* phase appeared and soon vanished into the fluid performing wavy motions. Figure 9(*i*) (plate 3) is an example of this phase (also named the *hole* phase). During these motions the cloud became gradually sparse and entered the *final* phase, where active convection was observed. In most cases transitions from one phase to another took place suddenly, and each phase, even when it had a short lifetime, could be recognized clearly. No phase seemed to be much modified by the preceding phase.

Top and side views of the *hole* and *wave* phases are shown in figures 10(*a*) and (*b*) (plate 3) respectively. The cloud is seen to occupy the lower part of the layer, while the upper part is clear.

The duration of each phase was not unique for each experimental run, but the whole process usually finished within a few minutes, five at most.

	D_m (cm²/s)	κ (cm²/s)	κ^g (cm²/s)
Air	—	0·21	—
Water vapour	0·26	0·46	0·22
Methanol vapour	0·16	0·25	0·22
Ethanol vapour	0·12	1·7	0·23

TABLE 1. Values of D_m (through air), κ (thermal diffusivity in pure substance) and κ^g (in air saturated with vapour), each at 30 °C

7.2. *Measurement of R_c, R_h, etc.*

The critical values R_c and R_h have been obtained by observing the appearances of the *cellular* and *hole* phases respectively. The results (figure 11) show that $R_c = 1800 \pm 50$ and $R_h = 1400 \pm 50$. In the same figure is shown a result for dry-air convection, from which we have the critical value 1800. It is a little higher than the theoretical value 1708, but this discrepancy may be due to errors in the measurement of R. Note that convective motions must be visible at values of R larger than the theoretical one. The critical value of R for the appearance of the *wave* phase has not been measured, for it was difficult to recognize the critical condition for the wavy motion.

The motions in the *cellular*, *wave* and *hole* phases had nearly the same horizontal scale, about twice the thickness d. In particular the scale of the holes was measured when the convection pattern was regular. When $R = 2{\cdot}1 \times 10^3$, an average distance between the opposite sides of the hexagons was $(2{\cdot}1 \pm 0{\cdot}1)d$.

By using a video tape recorder the speed of travelling waves in the *wave* phase was measured for the two cases $R = 3{\cdot}6 \times 10^3$ ($d = 1{\cdot}2$ cm) and $R = 5{\cdot}2 \times 10^3$ ($d = 1{\cdot}4$ cm). The speed increased with time and reached a maximum value of 0·8 cm/s in both cases, but after a while it seemed to cease increasing.

7.3. *Alcohol clouds*

In order to examine the dependence on the diffusion coefficients D_m and κ^g, we studied two further composite fluids, made using methanol or ethanol (alcohol clouds). For the water cloud described in the previous section, the parameter Q, defined in (34) with (31), is positive ($\approx +0{\cdot}01$ at 10° C) because of the inequality $D_m > \kappa^g$ (see table 1), while for both alcohol clouds Q is negative because $D_m > \kappa^g$. On the other hand, in every experiment heated from below ($a > 0$), the parameter S in (34) is positive because natural sedimentation of droplets yields positive b. Thus in the experiments on alcohol clouds it is plausible that the stability boundary at $S = Q$ (< 0) in the R, S plane (figure 2) does not come into play in practice.

For almost all the observations of alcohol clouds we found one of the following series of phases: *initial* → *static* → *final* or *initial* → *wave* → *static* → *final*. Sometimes a motion similar to the *cellular* phase occurred while the *hole* phase was not observed. Thus we infer some relation between the instability in region I and the *hole* phase.

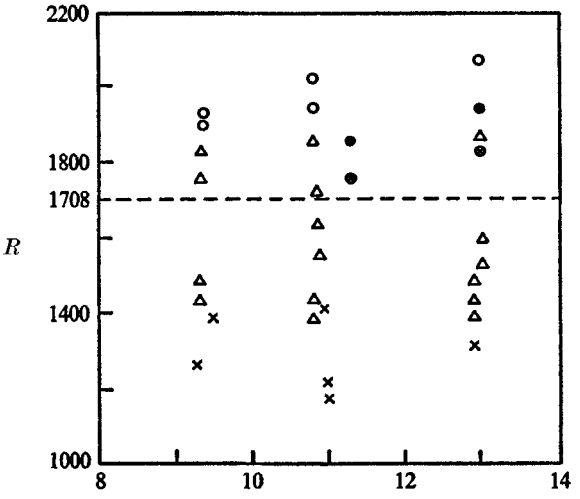

FIGURE 11. Measured values of R for various values of d. ○, onset of the cellular phase; △, onset of the hole phase with no cellular phase; ×, no hole phase; ●, onset of cellular convection in the dry air; ⊗, no convection in dry air.

8. Discussion

Here we show that the observed phenomena (summarized in figure 8) can be well predicted by the theory by means of an R, S diagram (figure 2). A sequence of several phases observed in each experimental run is considered to be caused by variation of S with an almost constant value of the Rayleigh number R. First we consider the water cloud.

We have no measured estimate of S except that of 0·5 for the *wave* phase (see below). However in the *initial* phase we may assume S to be much less, since the droplet distribution will be more uniform owing to disturbances due to the smoke injection or some convective motions before injection. Therefore the initial position of the state point in the R, S plane lies nearer the R axis and to its right-hand side, but may be on either side of the line $S = Q$. If it lies to its right, we can ascribe the appearance of the *cellular* phase following the initial phase to the instability in region II of figure 2. This is an oscillatory mode, whose frequency increases from zero on the line $S = Q$ with increasing S at fixed R (figure 4). When S is small enough, i.e. when the frequency is small, the mode will be almost steady. The system enters a *wave* phase corresponding to the oscillatory mode (for large enough R, see below) as S increases further. On the other hand, if the state point lies to the left of the line $S = Q$, another mode of instability may emerge. However, it appears to be highly possible that, before this mode amplifies enough, the state point moves, crossing the line $S = Q$, when we consider the facts that the value of Q is as small as $O(10^{-2})$ and that the characteristic time of growth of a disturbance for $R = 1500$ and $S = 0$, which is $d^2/\hat{\kappa} \approx 5$ s in our case (§4.2), is not so small compared with the characteristic time of sedimentation of about

30 s. In any case, the critical Rayleigh number for the appearance of convective motion following the *initial* phase would be equal to that of the mode of instability in region II, which is $R_A = 1725$ in figure 4. This agrees quite well with the minimum Rayleigh number R_c (≈ 1800) for the appearance of the *cellular* phase. It is worthwhile to note that the instability in region II is a modified version of the instability mode in single-component thermal convection.

When R is less than R_A, the state point stays in the stable region III (figure 2), which corresponds to the *static* phase. In this phase, however, sedimentation is going on, and the parameter S first increases and then decreases after attaining a certain maximum. The state point turns back again to the left and finally enters region I, which has an instability mode. We regard this as the *hole* phase. However in the experiment we found no convective motion for $R < R_h$ (≈ 1400). The explanation is as follows: the maximum growth rate $\sigma_r^{(m)}$ is less than unity for $R < 1400$ (figure 6), therefore the characteristic time of growth of a disturbance is more than 5 s, which is comparable with the fading-out time of the cloud. After the disappearance of the cloud, the composite fluid will become a two-component fluid, which will be inert and behave differently, and its critical Rayleigh number will be larger (if the vapour diffusion is neglected, the critical value should be 1708).

When R is larger than R_A ($\approx R_c$), the *wave* phase follows the *cellular* phase as described above. As S increases further, the state point enters the stable region III and the *wave* phase becomes the *static* phase. However when R is only slightly larger than R_c, i.e. when the growth rate σ_r is small, the *wave* phase does not emerge. Probably the system enters the stable region III without having enough time for amplification of wavy disturbances. When the state point turns back to the left inside region III and re-enters region II, the *wave* phase should follow the *static* phase. But its appearance was not observed even for larger R. The system does not seem to have enough time to amplify wavy disturbances, and instead it enters the *hole* phase, which appears when the calm cloud layer settles into a thin layer just above the bottom. In this phase non-oscillatory disturbances grow up and regular patterns of convection cells are seen. Finally this becomes a transparent *final* phase.

According to the observations at very high R, the *static* phase does not emerge. This can be explained by assuming that S does not become larger than a certain value $O(1)$, so that the state point turns back, remaining inside region II, for such a high R. This assumption can be confirmed by a measured estimate of S in the *wave* phase. Normalizing the measured maximum wave speed c and wavenumber k by $\hat{\kappa}/d$ and d^{-1} respectively, we have $\sigma_i\,(= kc) \simeq 15$ or 20 for $R = 3600$ or 5200 respectively. By looking at figure 4 we obtain $S \sim 0{\cdot}5$ for both cases.

The theoretical value of the wavelength of the most unstable mode in the rigid-wall case is 1·9 for $R \approx 2000$ and $S = 0$. Agreement with the measured wavelength in the *hole* phase is rather good. In the *wave* and *static* phases, we can observe a clear upper surface of the cloud layer as is shown in figures 10(*a*) and (*b*), so that the droplet distribution would be rather discontinuous. Hence the linear distribution assumed in the theory would be a very rough representation.

Interpretations of phenomena in alcohol clouds are also possible on the same lines as above, taking account of the fact that the line $S = Q$ lies to the left of the

R axis in R, S plane. Therefore the *hole* phase does not appear in alcohol clouds before the *final* phase.

In conclusion, all the qualitative features of our experiments have been explained in terms of the theory summarized in §5. The mechanism of evaporation and subsequent diffusion presented there must be taken into consideration when we investigate thermal convection in the three-component fluid, and the dependence of the phenomena on the parameter Q is crucial.

Our results may be applied to various meteorological phenomena so long as diffusion processes are important, although their application must be subject to the many restrictions made in the analysis. Here it may be interesting to refer to a phenomena called 'hole-in-cloud' reported in *Weatherwise* (vol. 4, 1968, frontispiece), which is a hole of diameter 10 kilometres in a cloud layer of height several kilometres. The present authors are inclined to regard it as a kind of convective motion caused by a thermal instability in which vapour condensation (or ice formation) and vapour diffusion play an important role. This opinion agrees with one of the interpretations of this phenomenon (Agee 1969). For the strict analysis of phenomena in the atmosphere, assumption (a) in §1 must be removed.

The authors would like to express their gratitude to Professor I. Imai and Professor H. Hasimoto for their encouragement throughout this work. They are also grateful to Dr J. S. Turner, who read the manuscript and gave useful, constructive criticism.

Appendix A

When the diffusion of small (liquid) droplets is caused by Brownian motion in a medium, the coefficient of diffusion D^d is given by the Einstein relation

$$D^d = \zeta k_B T,$$

where T is the temperature of the medium, k_B the Boltzmann constant and ζ the mobility of the Brownian 'particle'. For a spherical droplet with radius a, the Stokes drag law gives $\zeta = 1/6\pi\mu a$, where μ is the fluid viscosity. Thus one obtains $D^d = k_B T/6\pi\mu a$. Hence $D^d = 1{\cdot}2 \times 10^{-7}\,(\mathrm{cm}^2/\mathrm{s})$ for a particle with $a = 10^{-4}$ cm in air at $T = 300°$ K. The ratio of D^d to κ^g or D_m is about 10^{-6}, so that one may neglect the diffusion of droplets in the present problem.

If the diffusivity of the droplets is taken into account, (3), (30c) and (40) must be replaced by

$$\frac{D}{Dt}r = -\frac{1+r}{\rho^g}\eta + D^d\nabla^2 r, \tag{A 1}$$

$$\partial r_1/\partial t = bw + \beta\nabla^2 T_1 + D^d\nabla^2 r_1, \tag{A 2}$$

$$N^2\sigma^3 + (1+P+K_r)N^4\sigma^2 + \{(P+K_r+PK_r)N^6 - (R-R_s)Pk^2\}\sigma + PK_rN^8 + \{(1-K)R_s - K_rR\}Pk^2N^2 = 0, \tag{A 3}$$

respectively, where $K_r = D^d/\hat{\kappa}$ and $R_s = SR$. When $K_r = 0$, (A 3) reduces to (40) while if $K = 0$ it reduces to the equation for the double-diffusive system (Turner 1973, equation (8.1.8)).

The boundary between stability and instability is represented by two curves (branches of two hyperbolas) in S, R plane as follows:

$$R = \frac{(1+P)(1+K_r)(1+K_r/P)}{1+P-Q-(P+K_r)S} R_0 \quad \text{for} \quad S > S_0, \tag{A 4}$$

$$R = \frac{K_r}{K_r+Q-S} R_0 \quad \text{for} \quad S < S_0, \tag{A 5}$$

where $$S_0 = \frac{(1+P)(1+K_r)(Q+K_r)(P+K_r) - K_r(1+P-Q)}{(1+P+K_r)(P+K_r)}.$$

These curves meet at a point on the line $S = S_0$. The imaginary part of σ does not vanish on the curve (A 4), while it does vanish on (A 5). It is worth noting that, when $K_r = 0$, one obtains $S_0 = Q$ and (A 4) reduces to (42) with N^6/k^2 in (42) replaced by R_0, and that for $S < S_0$ there is a non-zero critical Rayleigh number in this case, which, however, vanishes for $K_r = 0$ (the case discussed in the main body of the present paper).

Appendix B

Under the conditions $S < Q < 1$, $0 < R$ and $0 < P$, one can show that σ_r should be negative provided that σ_i does not vanish. Equations (33) can be written in the form

$$(D^2 - \sigma/P) D^2 W = -Rk^2(A\sigma^{-1}D^2\Theta - B\Theta), \tag{B 1}$$

where $A = Q-S\,(>0)$ and $B = 1-S\,(>0)$. Multiplying (B 1) by $\overline{W}$ (the complex conjugate of W) and integrating over z, one obtains

$$\int_0^1 \overline{W} D^2 \left(D^2 - \frac{\sigma}{P}\right) W dz = -Rk^2 \int_0^1 \overline{W} \left(\frac{A}{\sigma} D^2\Theta - B\Theta\right) dz. \tag{B 2}$$

Using (33b) on the right-hand side, integrating both sides by parts and using the boundary conditions (36), one obtains

$$\int_0^1 \left\{ |W''|^2 + \left(2k^2 + \frac{\sigma}{P}\right)|W'|^2 + k^2\left(k^2 + \frac{\sigma}{P}\right)|W|^2 \right\} dz$$
$$= Rk^2 \left[A \frac{\overline{\sigma}}{|\sigma|^2} \int_0^1 \{|D^2\Theta|^2 + \overline{\sigma}(|\Theta'|^2 + k^2|\Theta|^2)\} dz \right.$$
$$\left. + B \int_0^1 \{|\Theta'|^2 + (k^2+\overline{\sigma})|\Theta|^2\} dz \right]. \tag{B 3}$$

It should be noted that (B3) is valid for both free and rigid bounding surfaces. Writing $\sigma = \sigma_r + i\sigma_i$ and equating the imaginary parts on both sides of (B 3), one has

$$\sigma_i \left[\frac{1}{P} \int_0^1 \{|W'|^2 + k^2|W|^2\} dz + Rk^2 B \int_0^1 |\Theta|^2 dz \right.$$
$$\left. + Rk^2 \frac{A}{|\sigma|^2} \int_0^1 \{|D^2\Theta|^2 + 2\sigma_r(|\Theta'|^2 + k^2|\Theta|^2)\} dz \right] = 0, \tag{B 4}$$

hence $\sigma_r < 0$ if $\sigma_i \neq 0$.

REFERENCES

AGEE, E. M. 1969 *Weatherwise*, **22**, 19.
BAINES, P. G. & GILL, A. E. 1969 *J. Fluid Mech.* **37**, 289.
HADLOCK, R. K. & HESS, S. L. 1968 *J. Atmos. Sci.* **25**, 161.
MARBLE, F. E. 1969 *Astron. Acta*, **14**, 585.
SCHECHTER, R. S., PRIGOGINE, I. & HAMM, J. R. 1972 *Phys. Fluids*, **15**, 379.
SCHWIDERSKI, E. W. & SCHWAB, H. J. A. 1971 *J. Fluid Mech.* **48**, 703.
SPARROW, E. M., GOLDSTEIN, R. J. & JONSSON, V. K. 1964 *J. Fluid Mech.* **18**, 513.
SPIEGEL, E. A. & VERONIS, G. 1960 *Astrophys. J.* **131**, 442.
STERN, M. E. 1960 *Tellus*, **12**, 172.
STOMMEL, H., ARONS, A. B. & BLANCHARD, D. 1956 *Deep-Sea Res.* **3**, 152.
TRITTON, D. J. & ZARRAGA, M. N. 1967 *J. Fluid Mech.* **30**, 21.
TURNER, J. S. 1963 *Quart. J. Roy. Met. Soc.* **89**, 62.
TURNER, J. S. 1973 *Buoyancy Effects in Fluids*, chap. 8. Cambridge University Press.
TURNER, J. S. & YANG, I. K. 1963 *J. Fluid Mech.* **17**, 212.
VERONIS, G. 1965 *J. Mar. Res.* **23**, 1.
WOLLKIND, D. J. & FRISCH, H. L. 1971 *Phys. Fluids*, **14**, 13.
YANG, I. K. 1968 *Proc. Int. Conf. on Cloud Physics, Toronto*, p. 529.

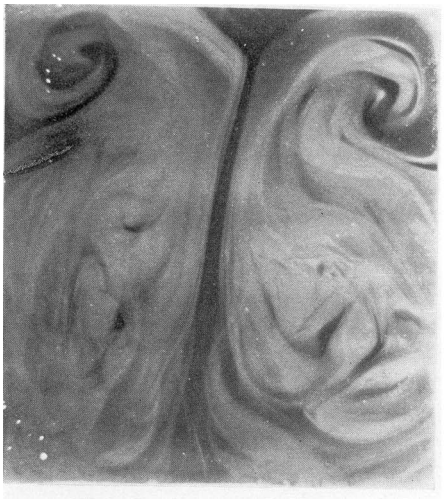

(*a*)

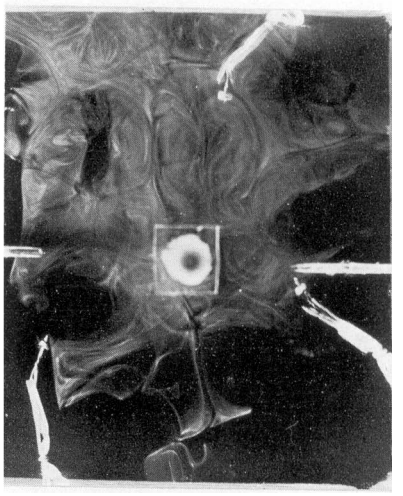

(*b*)

(*c*)

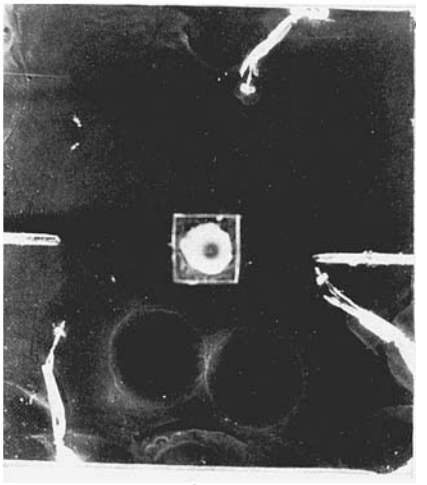

(*d*)

FIGURES 9 (*a–d*). For legend see plate 3.

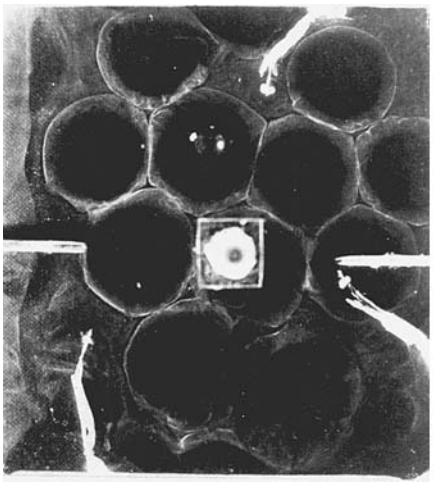

(*e*)

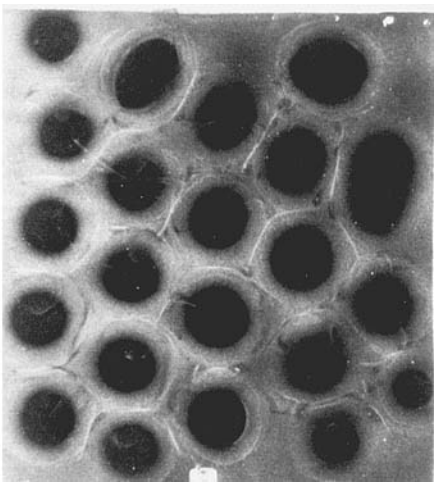

(*f*)

(*g*)

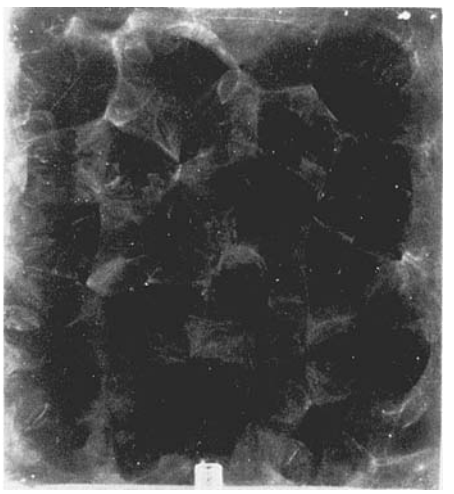

(*h*)

FIGURES 9 (*e–h*). For legend see plate 3.

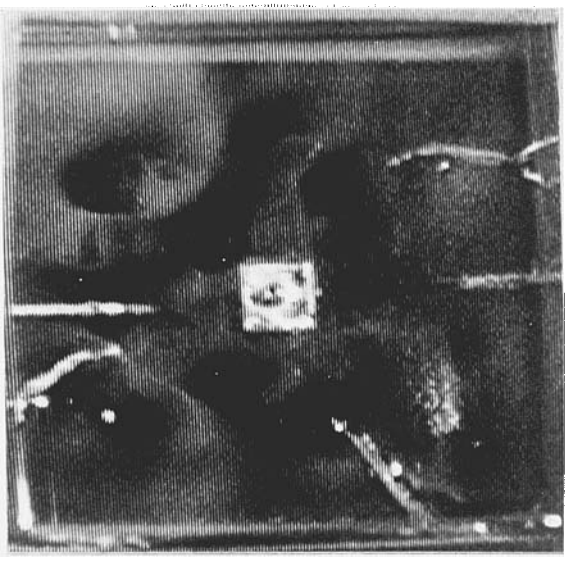

(*i*)

FIGURE 9. Top views of several phases. Descriptions of these phases are given in §7.1. (*a*) *Initial* phase, $R = 1{\cdot}6 \times 10^3$. (*b*) *Cellular* phase, $R = 2{\cdot}0 \times 10^3$. (*c*) *Wave* phase, $R = 3{\cdot}5 \times 10^3$. A few holes near a side wall are produced because of non-uniformity of the cloud distribution in the horizontal direction. (*d*) Earlier stage of the *hole* phase, $R = 2{\cdot}0 \times 10^3$. (*e*) *Hole* phase, $R = 2{\cdot}0 \times 10^3$. (*f*) *Hole* phase, $R = 3{\cdot}5 \times 10^3$. (*g*) *Final* phase, $R = 1{\cdot}6 \times 10^3$. (*h*) *Final* phase, $R = 3{\cdot}5 \times 10^3$. (*i*) Isolated holes in the turbulent waves, $R = 5{\cdot}2 \times 10^3$. The small black point in the centre of the photographs (*b*), (*d*), (*e*) and (*i*) is the pipe *J*. The five white lines extending from the perimeter in the same photographs are the thermocouples *K* connected in series.

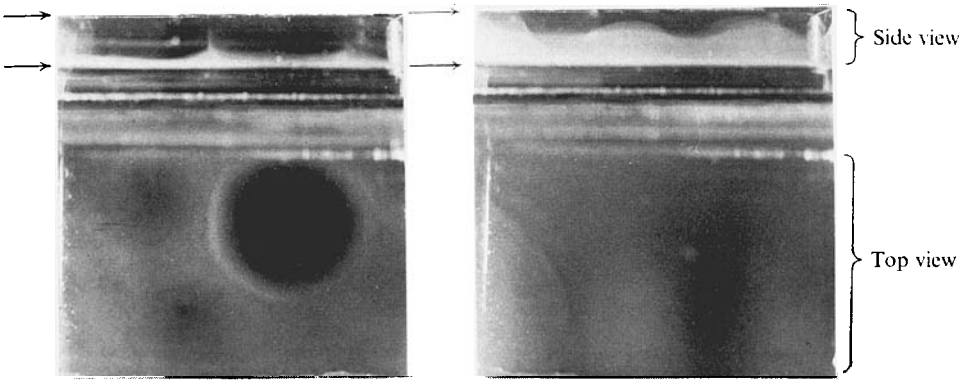

(*a*) (*b*)

FIGURE 10. Top and side views of (*a*) a hole and (*b*) waves in the smaller convection chamber. Arrows in the side views show the upper and the lower boundaries of the convection layer.